Journal of Solid State Chemistry 184 (2011) 379–386

Contents lists available at ScienceDirect

Journal of Solid State Chemistry

journal homepage: www.elsevier.com/locate/jssc

Dicarboxylate assisted synthesis of the monoclinic heterometallic tetrathiocyanato bridged copper(II) and mercury(II) coordination polymer $\{Cu[Hg(SCN)_4]\}_n$: Synthesis, structural, vibration, luminescence, EPR studies and DFT calculations

Ali Akbar Khandar [a,*], Axel Klein [b], Akbar Bakhtiari [a,b], Ali Reza Mahjoub [c], Roland W.H. Pohl [b]

[a] Department of Inorganic Chemistry, Faculty of Chemistry, University of Tabriz, 5166614766 Tabriz, Iran
[b] Institut für Anorganische Chemie, Universität zu Köln, Greinstraße 6, 50939 Köln, Germany
[c] Department of Chemistry, School of Science, Tarbiat Modares University, P.O. Box 14155-4838 Tehran, Iran

ARTICLE INFO

Article history:
Received 20 August 2010
Received in revised form
29 November 2010
Accepted 6 December 2010
Available online 10 December 2010

Keywords:
Coordination polymer
Copper(II)
Mercury(II)
Thiocyanate
Luminescence
DFT

ABSTRACT

The synthesis of the monoclinic polymorph of $\{Cu[Hg(SCN)_4]\}_n$ is reported. The compound, as determined by X-ray diffraction of a twinned crystal, consists of mercury and copper atoms linked by $\mu_{1,3}$-SCN bridges. The crystal packing shows a highly porous infinite 3D structure. Diagnostic resonances for the SCN^- ligand and metal–ligand bonds in the IR, far-IR and Raman spectra are assigned and discussed. The electronic band structure along with density of states (DOS) calculated by the DFT method indicates that the compound is an indirect band gap semiconductor. The DFT calculations show that the observed luminescence of the compound arises mainly from an excited LLCT state with small MLCT contributions (from the copper to unoccupied π^* orbital of the thiocyanate groups). The X-band EPR spectrum of the powdered sample at room temperature reveals an axial signal with anisotropic g factors consistent with the unpaired electron of Cu(II) ion in the $d_{x^2-y^2}$ orbital.

1. Introduction

Research on the design and synthesis of crystalline coordination polymers is an active topic in current chemistry [1,2]. With regard to the possible correlation between structure and function [3–8], coordination polymers have gained attraction as promising materials of the future [9] with specifically tailored, useful properties, such as magnetism [10,11], electrical conductivity [12], non-linear optical behavior [13,14], luminescence [15,16], porosity and gas storage [17,18], or drug delivery [19].

Recently, the synthesis and structural characterization of multidimensional homo- and heterometallic coordination polymers based on the pseudo-halides OCN^- [20,21], SCN^- [22–25], $SeCN^-$ [26] and N_3^- [27–30] has been in the focus of many research groups worldwide. This interest is based not only on the high versatility of their binding modes which are end-on-η^1(N), end-on-η^1(X), bridging-η^1(N)–η^1(X), bridging-μ–η^1(N), bridging-μ–η^1(X) and combinations of these and allow a rich architectonical diversity in corresponding structures, but also on their exceptional potential applications. The thiocyanate ligand with its marked ambidentate character and all the versatile coordination modes described above is expected to afford a number of homo- and heterometallic discrete one-, two- and three-dimensional structural assemblies with specific structural features and optical and magnetic properties [31–34]. Simultaneous presence of two different metal centers can potentially give rise to interesting physico-chemical properties and lead to attractive novel topologies and intriguing frameworks. However, despite the various coordination modes of the SCN^- group to the metal ions, it is not widely used in the design and synthesis of inorganic compounds and the heterometallic thiocyanato bridged species are comparatively less numerous [34].

The series of coordination polymers, $M[Hg(SCN)_4]$ containing M=Zn, Cd, Cu, Ni, Co, Fe, or Mn have been investigated for more than a century, already in 1901 their characteristic shapes and colors have been described [35]. In 1970, Bell Telephone Laboratory reported that the $Cd[Hg(SCN)_4]$ and $Zn[Hg(SCN)_4]$ crystals are very effective second harmonic generating (SHG) materials for doubling the frequency of a Nd:YAG 1064 nm laser to generate 532 nm green laser light [36]. Since then, crystal growth methods and mechanism, physical and nonlinear optical properties of the $M[Hg(SCN)_4]$ (M=Zn, Cd, Co, Fe, Mn) series have been described in detail (see for example [37–43]). Moreover, the semiconducting properties of an orthorhombic $\{Cu[Hg(SCN)_4]\}_n$ [44–47] and the tetragonal $(Cu_xZn_{1-x})[Hg(SCN)_4]$ ($0<x<0.22$) [48] have been previously described [45].

On the other hand, anions and counter anions have been shown to have key effects on the structure of the final product [49,50]. They

* Corresponding author. Fax: +98 411 3340191.
E-mail address: akhandar@yahoo.com (A.A. Khandar).

0022-4596/$ - see front matter © 2010 Elsevier Inc. All rights reserved.
doi:10.1016/j.jssc.2010.12.012

can control the topology of the coordination architectures in two ways: (a) influencing the coordination sphere of the metal ions and so the connectivity of the framework by the coordinating ability of the anions and (b) stabilizing the coordination framework by supramolecular interactions such as hydrogen bonding to host framework or lattice solvents. The coordination flexibility of copper(II) ions coupled with the possible presence of carboxylates can lead to the formation of different assemblies, spanning from mononuclear complexes to supramolecular coordination polymers or metal-organic frameworks [51]. Malonates in association with late 3*d* transition metals, have been demonstrated to provide a wealth of coordination modes to the *M*(II) ions and several coordination polymers with a distinct binding to Cu(II) ions [52,53]. In the current research work, we demonstrate that malonates (as mono- and di-anions of propane dicarboxylic acid) are potential candidates for crystal growth without entering the final product.

In this context, we sought to reexamine the chemistry of $[M(SCN)_4]^{2-}$ building blocks in particular as the potential ligands for new coordination polymers. Herein, we will report the synthesis and X-ray structure determination of the monoclinic $\{Cu[Hg(SCN)_4]\}_n$. Moreover, the IR, far-IR, Raman, photoluminescence as well as EPR spectra of the compound will be discussed. Also, the emission and semiconducting behavior of the compound will be illustrated through the density functional theory calculation of electronic band structure along with density of states.

2. Experimental section

2.1. Materials and methods

All chemicals were commercially purchased and used without further purification. Elemental analysis (C, H, N and S) was carried out on a Hekatech CHNS EuroEA 3000 Analyzer. Infrared (IR) spectra (4000–50 cm^{-1}) were recorded using a Bruker IFS66vS spectrometer. Raman spectra were obtained from a powder sample using a Bruker FRA106S spectrometer. Luminescence spectra of a solid powder sample were recorded on a Spex FluoroMax-3 UV/Vis emission spectrophotometer (equipped with a Xe lamp). The excitation wavelengths were 425, 462 and 511 nm according to the bands observed in excitation spectra. EPR spectra were recorded on powder samples at room temperature in the X band on a Bruker ELEXSYS 500E instrument. Single-crystal X-ray diffraction data were collected using graphite-monochromatized Mo*K*α radiation (λ=71.073 pm) on a IPDS I (STOE and Cie.) at 293(2) K.

2.2. Synthesis of monoclinic $\{Cu[Hg(SCN)_4]\}_n$

Malonic acid (0.1041 g, 1 mmol) dissolved in 1 mL of 1 M aqueous solution of NaOH was added to a solution of copper(II) chloride dihydrate (0.1705 g, 1 mmol) in 24 mL of methanol. This solution was added to a solution of mercury(II) thiocyanate (0.3168 g, 1 mmol) in 25 mL of methanol. The resulting greenish blue solution was stirred for 15 min, filtered and left at room temperature for crystallizing. After 1 week, black-green crystals of $\{Cu[Hg(SCN)_4]\}_n$, suitable for X-ray diffraction were obtained (yield: ca. 0.214 g, 43% based on $CuCl_2 \cdot 2\,H_2O$). Anal. Calcd. for $C_4N_4S_4CuHg$ (%): C, 9.68; N, 11.29; S, 25.83%; Found: C, 9.68; N, 10.98; S, 26.01%.

The same compound (as determined by XRD) was also obtained in a different manner: A solution of copper(II) acetate monohydrate (0.1997 g, 1 mmol) and malonic acid (0.1041 g, 1 mmol) in 40 mL of distilled water was heated while stirring and thus reduced to ca. half of the volume. The resultant copper(II) malonate solution, cooled down to room temperature, was added to a solution of mercuric thiocyanate (0.3168 g, 1 mmol) in 20 mL of methanol while stirring at room temperature. The obtained greenish blue solution was filtered and left undisturbed for crystallizing (yield: ca. 0.223 g, 45% based on copper(II) acetate monohydrate). Anal. Calcd. for $C_4N_4S_4CuHg$ (%): C, 9.68; N, 11.29; S, 25.83%; Found: C, 9.66; N, 11.23; S, 25.80%.

2.3. X-ray data collection, structure solution and refinement

The suitable crystal of the compound was isolated as described above and mounted in sealed glass capillaries on a Stoe IPDS I single crystal diffractometer (T=293(2) K, Mo*K*α radiation). For data collection and reduction the Stoe program package [54] was applied. The structural analysis was complicated because of twinning. The obtained cell was checked by analyzing of the diffractions on the base of Yvon LePage's algorithm [55] provided in PLATON [56]. The structure was solved using direct methods and refined on F^2 by full-matrix least squares technique [57] within WINGX [58]. The twin law was extracted by analyzing of poorly fitting intensity data provided by ROTAX program [59]. The final refined structure was checked with the ADDSYM algorithm in the program PLATON [56] and no higher symmetry was found. The BASF parameter was refined to 0.50856. All atoms were refined anisotropically. A summary of crystal data and refinement results is provided in Table 1. The available data for the orthorhombic $\{Cu[Hg(SCN)_4]\}_n$ [46] are also given for comparison.

3. Computational details

The crystallographic data of the compound determined by X-ray were used to calculate its electronic band structure along with density of states (DOS), by density functional theory (DFT) using

Table 1
Crystal data and structure refinement information of monoclinic $\{Cu[Hg(SCN)_4]\}_n$. Corresponding data for the orthorhombic polymorph is given for comparison.

complexes	Monoclinic $\{Cu[Hg(SCN)_4]\}_n$	Orthorhombic $\{Cu[Hg(SCN)_4]\}_n$
Empirical formula	$C_4CuHgN_4S_4$	$C_4CuHgN_4S_4$
M (g mol^{-1})	496.50	496.50
T (K)	293(2)	
Crystal system	Monoclinic	Orthorhombic
Space group	*C*2/*c*	*Pbcn*
a (Å)	9.0084(18)	9.03
b (Å)	7.6993(19)	7.68
c (Å)	15.1560(20)	15.15
β (deg)	90.000(10)	90
V (Å^3)	1051.2(4)	
Z	4	4
Crystal size (mm)	0.16 × 0.14 × 0.10	
F (000)	900	
D_{calc} (Mg/m^3)	3.137	
μ (Mo*K*α) (mm^{-1})	17.364	
hkl range	$-11 \le h \le 7$ $-10 \le k \le 6$ $-19 \le l \le 19$	
Refl. collected	2513	430
Independent refl.	1266	
No. of parameters	70	
$\Delta(\rho)$ (e Å^{-3})	1.418 and −1.137	
GOF	0.815	
R[a]	0.0352 0.0610[b]	
wR[a]	0.0640 0.0696[b]	

[a] $R=\sum\|F_o|-|F_c\|/\sum|F_o|$, $wR_2=[\sum(w(F_o^2-F_c^2)^2/\sum(w(F_o^2)^2]^{1/2}$; $[F_o > 4\sigma(F_o)]$.
[b] Based on all data.

one of the three non-local gradient-corrected exchange-correlation functionals (GGA-PBE). Calculations were performed with the CASTEP code [60,61], which uses a plane wave basis set for the valence electrons and norm-conserving pseudopotential [62] for the core electrons. The number of plane waves included in the basis was determined by a cutoff energy E_c of 550 eV. Pseudoatomic calculations were performed for C-$2s^2 2p^2$, N-$2s^2 2p^3$, S-$3s^2 3p^4$, Cu-$3d^{10} 4s^1$ and Hg-$5d^{10} 6s^2$. The parameters used in the calculations and convergence criteria were set by the default values of the CASTEP code, e.g., reciprocal space pseudopotentials representations, eigen-energy convergence tolerance of 1×10^{-6} eV, Gaussian smearing scheme with the smearing width of 0.1 eV, and Fermi energy convergence tolerance of 1×10^{-7} eV.

4. Results and discussion

4.1. Synthesis

The reaction of $Hg(SCN)_2$ and copper(II) chloride in the presence of malonic acid mono-deprotonated by NaOH or the reaction of $Hg(SCN)_2$ and copper(II) malonate, results in the monoclinic polymorph of $\{Cu[Hg(SCN)_4]\}_n$ in contrast to the previously described reaction of $K_2[Hg(SCN)_4]$ and copper(II) salts of simple anions such as sulfate, which results in the formation of the orthorhombic variant $\{Cu[Hg(SCN)_4]\}_n$ [45]. So, it may be suggested that the malonates could control the formation of the crystal structure without entering the final product. Based on the HSAB concept a rational explication would be that while in solution both the malonate ligands and the SCN^- ligands were coordinated to copper, during the crystallization process the hard donor oxygen atoms of the malonate ligand were completely substituted by the softer thiocyanate nitrogen atoms.

The X-ray structure analysis of different crystals obtained from recrystallizing the synthesized compound from different solvent systems (MeOH, MeOH/H_2O (1:1, v/v), MeOH/toluene (2:1, v/v) or acetone/H_2O (2:1, v/v)) reveal that the compound crystallizes inherently as twin crystals and no change of the polymorph was observed upon recrystallization. This could mean that the polymeric structure does not decompose completely by dissociation and the main structure is retained.

4.2. Description of crystal structure

X-ray analysis reveals that the compound has a three-dimensional framework, crystallizing in monoclinic space group $C2/c$ with $\beta = 90.000(10)^\circ$ (metrically orthorhombic unit cell [63]). Monoclinic structures with $\beta = 90^\circ$ are rare cases, but have been reported for a number of compounds (see for example [64–66]). Also, monoclinic structures with unique β angles very close to 90° are reported (see for example [67–69]). The asymmetric unit contains one Hg^{2+}, one Cu^{2+} and two SCN^- ions. The coordination mode of Hg^{2+} and Cu^{2+} ions is shown in Fig. 1. Selected bond lengths and angles are given in Table 2. For comparison, bond lengths and angles of the orthorhombic polymorph of $\{Cu[Hg(SCN)_4]\}_n$ [46] are given in brackets. The Hg atoms lie on two fold axes (Fig. 2), tetracoordinated to two S(1) and two S(2) atoms in a highly distorted tetrahedral geometry. The Hg(1)–S(1) and Hg(1)–S(2) bond lengths (2.497(3) and 2.655(3) Å, respectively), and the S(1)–Hg(1)–S(1) and S(2)–Hg(1)–S(2) bond angles (140.52(14)° and 94.05(14)°, respectively) are very similar to the values obtained for the orthorhombic $\{Cu[Hg(SCN)_4]\}_n$ [46]. The S(1)–Hg(1)–S(2) bond angles are 100.1(4)° and 106.5(4)°.

Fig. 3 illustrates the short contacts around Hg, S(2) and S(1) atoms. The highly distorted tetrahedral geometry around Hg atoms can be explained by additional short contacts of two

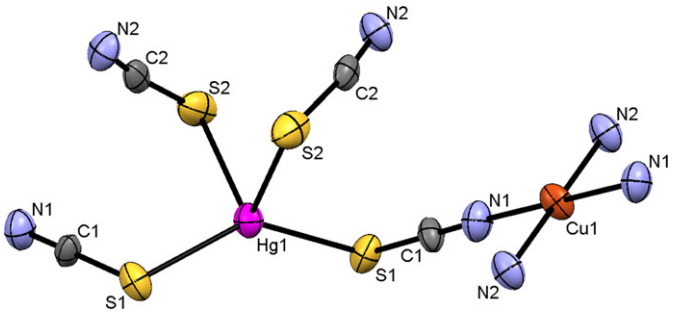

Fig. 1. The coordination environment of Hg and Cu atoms in the crystal structure with the numbering scheme. Atom displacement ellipsoids are shown at the 50% probability level.

Table 2
Selected bond lengths (Å) and angles (deg) and some geometrical parameters of the weak interactions[a] of monoclinic $\{Cu[Hg(SCN)_4]\}_n$. The available bond lengths and angles of the orthorhombic polymorph $\{Cu[Hg(SCN)_4]\}_n$ are also given in brackets for comparison.

Bond lengths			
Hg1–S1	2.497(3) [2.49]	Hg1–S2	2.655(3) [2.68]
Cu1–N1	1.959(10) [1.97]	Cu1–N2	1.938(11) [1.94]
S1–C1	1.768(17) [1.67]	S2–C2	1.88(2) [1.71]
C1–N1	1.198(14) [1.14]	C2–N2	1.165(16) [1.11]
Bond angles			
S1–Hg1–S1	140.52(14) [141]	S2–Hg1–S2	94.05(14) [94]
N1–Cu1–N1	180.0(6)	N2–Cu1–N2	180.000(1)
S1–Hg1–S2	100.1(4)	N2–Cu1–N1	89.7(5)
	106.5(4)		90.3(5)
Hg1–S1–C1	97.5(5) [100.5]	Hg1–S2–C2	89.2(5) [96]
Cu1–N1–C1	177.0(11)	Cu1–N2–C2	179.2(11)
N1–C1–S1	177.5(12)	N2–C2–S2	173.5(12)
Weak interactions			
Cu1···S1 (a,b)	3.014(3) [3.02]	Hg1···S2 (c,d)	3.279(3) [3.280]
S1···C1 (e)	3.50(1)	S1···C2 (c)	3.36(2)
S2···C1 (f)	3.28(2)	N1···C1(b)	3.12(2)
Weak interaction angles			
Cu1···S1–C1	95.1(5)	Cu1···S1···C1	99.6(3)
Cu1···S1···C2	92.3(3)	Hg1–S1···Cu1	138.2(3)
Hg1–S1···C1	118.4(3)	C1–S1···C2	172.2(5)
N1–Cu1···S1	91.6(3)	N2–Cu1···S1	95.9(4)
	88.4(3)		84.1(4)
S1···Cu1···S1	180.000(1)	Hg1–S2···Hg1	173.6(3)
S2–Hg1···S2	173.6(2)	S1–Hg1···S2	79.0(2)
	81.6(2)		76.8(2)
S2···Hg1···S2	103.1(2)	C2–S2···Hg1	89.6(5)
Hg1–S2···C1	126.1(3)	C2–S2···C1	124.7(5)
C1···S2···Hg1	59.3(2)	Cu1–N1···C1	87.9(4)
C1–N1···C1	89.4(8)	N1–C1···N1	90.6(8)
S1–C1···N1	88.5(5)		

[a] Symmetry transformation: (a) $\frac{1}{2}+x, \frac{1}{2}+y, z$; (b) $\frac{1}{2}-x, -\frac{1}{2}-y, -z$; (c) $-\frac{1}{2}+x, -\frac{1}{2}+y, z$; (d) $\frac{1}{2}-x, -\frac{1}{2}+y, \frac{1}{2}-z$; (e) $-x, -y, -z$; (f) $\frac{1}{2}-x, \frac{1}{2}+y, \frac{1}{2}-z$.

S(2) atoms (Hg(1)···S(2): 3.279(3) Å) from the neighboring $Hg(1)S(1)_2S(2)_2$ units (Fig. 3a). These two S(2)···Hg(1) short contacts with an angle of 103.1(2)° are *trans* to the two long Hg(1)–S(2) (2.655(3) Å) bonds, with an S(2)–Hg(1)···S(2) angle of 173.6(2)°. Each S(2) atom is also in short contact with the C(1) atom (Figs. 3b and 4) with a distance of 3.28(2) Å.

The Cu atoms lie on the centers of symmetry of the unit cell, located on (0, 1/2, 0) and symmetry related centers (Fig. 2). Each Cu atom is coordinated by two N(1) and two N(2) atoms in a regular planar square coordination geometry (Fig. 4), typical for a Cu(II) ion with a strong Jahn–Teller distortion, imposed by Cu(II) electronic configuration and crystal packing. Alternatively, the coordination geometry of the copper atoms could be described as a 4+2

octahedral geometry since two additional axial Cu(1)···S(1) (3.014(3) Å) weak interactions are observed. These two short *trans* contacts, with the contact angle of 180.000(1)°, are approximately perpendicular to the $CuN(1)_2N(2)_2$ plane with the bond angles of (91.6(3)°, 88.4(3)°) and (95.9(4)°, 84.1(4)°) for N(1)–Cu(1)···S(1) and N(2)–Cu(1)···S(1), respectively.

The *trans* and *cis* bond angles around the Cu atoms, in the $CuN(1)_2N(2)_2$ planes are (180.0(0)°, 180.000(1)°) and (89.7(5)°, 90.3(5)°), respectively. The structure exhibits Cu–N bond lengths of 1.959(10) and 1.938(11) Å.

The SCN^- groups are N-bonded to the Cu atoms in an approximately linear fashion (the C–N–Cu bond angles are 177.0(11)° and 179.2(11)°) and S-bonded to Hg atoms in a bent mode (the C–S–Hg bond angles are 97.5(5)° and 89.2(5)°). The geometrical parameters of the SCN^- groups linked to different metal atoms are 1.198(14) and 1.165(16) Å for C(1)–N(1) and C(2)–N(2) and 1.76(17) and 1.88(2) Å for S(1)–C(1) and S(2)–C(2) bond distances and 177.5 (12)° and 173.5(12)° for the S(1)–C(1)–N(1) and S(2)–C(2)–N(2) bond angles, respectively.

Each S(1)–C(1)–N(1) group is in weak interaction with the adjacent parallel S(1)–C(1)–N(1) group as shown in Fig. 4. This could be the reason why the S(1)–C(1) bonds are shorter than the S(2)–C(2) bonds and why the C(1)–N(1) bonds are longer than the C(2)–N(2) bonds. The distance of two Cu atoms in the Cu–N(1)–C(1)–S(1)···Cu units is 5.9252(9) Å.

Considering the direct bonds and the weak interactions, the S(1) surrounding could be described as a distorted trigonal bipyramid, as seen in Fig. 3c. In the equatorial positions, each S(1) atom is in weak interaction with one Cu(1) atom and one C(1) atom from the neighboring thiocyanate group. In the axial position, the S(1) atom is in short contact with one C(2) atom in the opposite direction to the S(1)–C(1) bond. Selected weak interactions and the related angles are also given in Table 2.

Viewing the crystal packing reveals that the Hg and Cu atoms are positioned in the planes perpendicular to the ***b***-axis (Fig. 2), bridged to

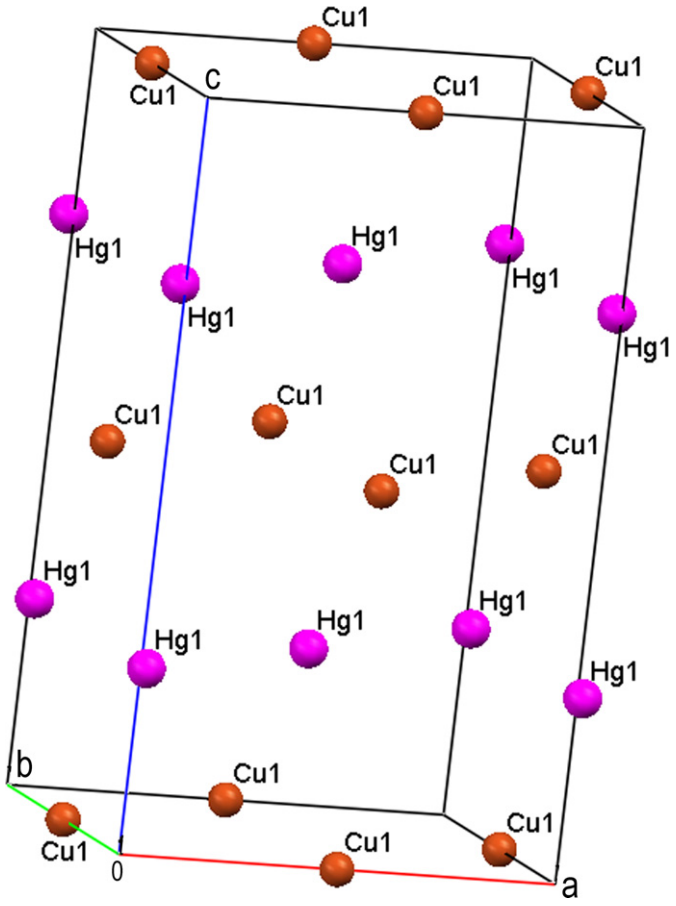

Fig. 2. The crystal packing of monoclinic $\{Cu[Hg(SCN)_4]\}_n$. The SCN^- groups are omitted for clarity.

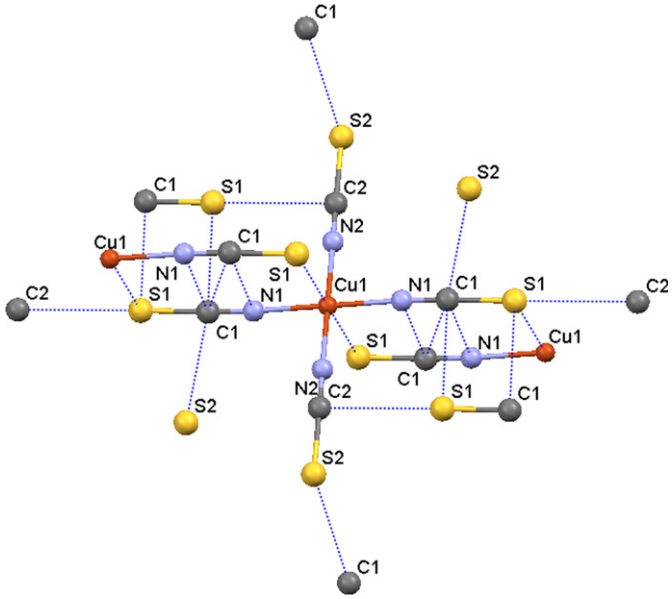

Fig. 4. Weak interactions of thiocyanate groups and short contacts to Cu atoms.

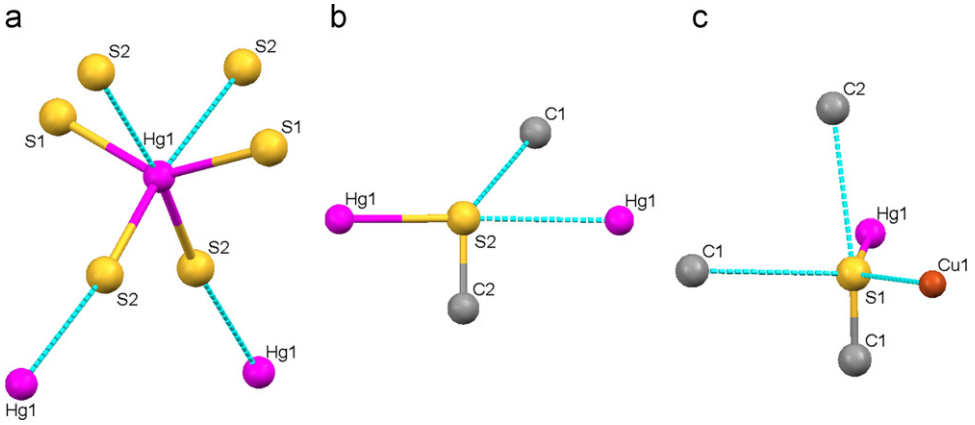

Fig. 3. Short contacts around (a) Hg, (b) S(2) and (c) S(1) atoms, illustrated by dashed lines.

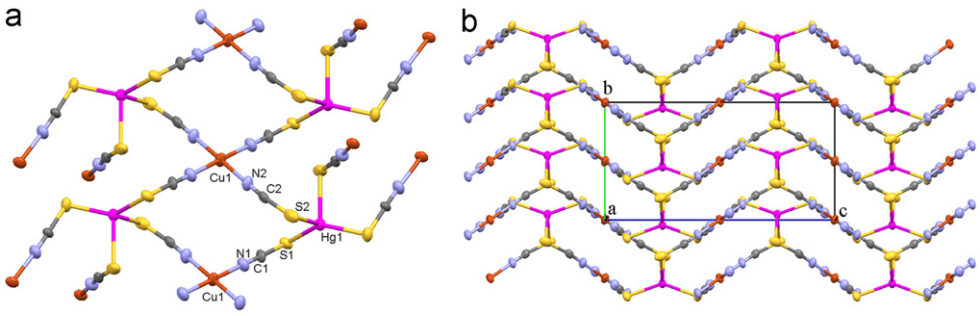

Fig. 5. (a) Curled square macrocycles formed by bridging of Cu and Hg atoms by two symmetrically nonequivalent thiocyanate groups and (b) the crystal packing viewed along the *a*-axis.

each other by the thiocyanate groups in the three dimensional space. Bridging of the Cu and Hg centers by two symmetrically nonequivalent thiocyanate groups, forms curled square macrocycles (Fig. 5a), connected to each other in the three dimensional space with the $[Hg(SCN)_4]^{2-}$ nodes as the secondary building units (SBUs) [70] and macrocycles as tertiary building units (TBUs) [51]. The Cu(1)…Cu(1) and Hg(1)…Hg(1) distances in the respective macrocycles are 5.9252(9) and 9.928(1) Å, respectively. Packing of these macrocycles along the [110] and [−110] directions results in rhombic channels, which turns to zigzag channels in the ***bc*** plane by viewing the crystal packing along the ***a***-axis (Fig. 5b). Analyzing of the Hg, S and Cu positions in the final structure, reveals *Cmcm* symmetry for the heavy atom positions.

4.3. Vibration spectra studies

It is a well-established criterion of infrared spectroscopy that $\nu_{CN} \geq 2100\ cm^{-1}$ indicates a thiocyanate bridge with a μ^2-1,3- or μ^3-1,1,3 bridging mode [71,72]. The ν_{CS} vibration lies between 860–780 cm^{-1} (N-bonding) and 720–690 cm^{-1} (S-bonding) and SCN bending vibration lies near 480 cm^{-1} (N-bonding) or 420 cm^{-1} (S-bonding) [73]. The strongest resonance in the IR spectrum of monoclinic $\{Cu[Hg(SCN)_4]\}_n$ appears at 2172 and 2155 cm^{-1}, characteristic of a ν_{CN} of a μ^2-1,3 bridging thiocyanate, comparable to the values 2170 and 2154 cm^{-1} observed for the orthorhombic polymporph [74–76]. This differs slightly to the resonances at 2134 and 2124 cm^{-1} for $K_2[Hg(SCN)_4]$ [74] and the single strong peak at 2053 cm^{-1} observed for KSCN [74,77]. The molecular symmetry requires the doubling of the ν_{CN} vibration for all the tetrahedral and polymeric octahedral compounds, since there are nonlinear SCN–*M*–NCS groups in the structure [78]. The weak absorption band at 798 cm^{-1} and very weak band at 763 cm^{-1} are assigned to CS stretching, indicating a shift to the higher energies compared to the corresponding ν_{CS} for KSCN observed at 746 cm^{-1} [74,77]. Compared to this, the respective CS stretching in the case of orthorhombic $\{Cu[Hg(SCN)_4]\}_n$ is reported to occur at 795 cm^{-1} [74–76]. The bending vibration modes of the SCN groups were observed at 463 and 436 cm^{-1} with the corresponding $2\delta_{SCN}$ occurred at 930 and 876 cm^{-1}, respectively. This is comparable with the values of orthorhombic $Cu[Hg(SCN)_4]$, for which the δ_{SCN} occurs at 459 and 437 cm^{-1} [74–76]. In contrast, the δ_{SCN} in the case of KSCN is observed at higher wavenumbers (486 and 471 cm^{-1}) [74,77].

The far-IR spectrum is given in Fig. 6. In the far-IR spectrum, the bands appeared at 320.13 and 285 cm^{-1} are assigned to the two Cu–N stretching modes as expected for a Cu–N_4 group in D_{2h} symmetry [76]. Also, a peak at 266 cm^{-1} appeared as a shoulder. The corresponding peaks for orthorhombic $\{Cu[Hg(SCN)_4]\}_n$ were observed at 318, 282 and 266 cm^{-1} [74–76]. The broad weak band, appearing as a shoulder at 215 cm^{-1}, is attributable to the Hg–S stretching mode. The highly distorted Hg–S_4 tetrahedron could be responsible to the corresponding weak band [76]. Interestingly, no

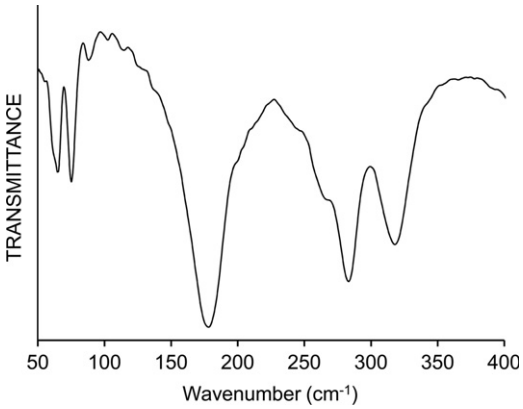

Fig. 6. The far-IR spectrum of monoclinic $\{Cu[Hg(SCN)_4]\}_n$.

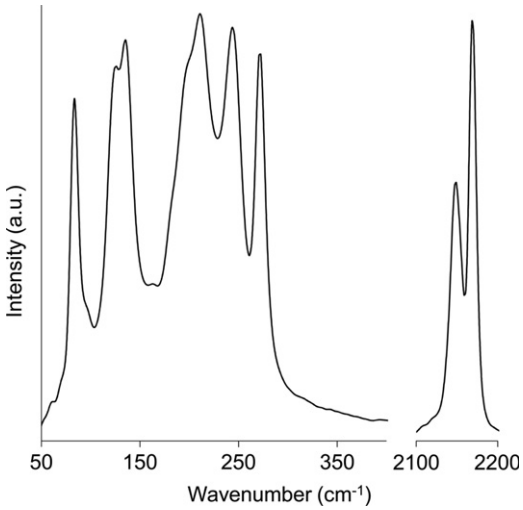

Fig. 7. The CN stretching region and 400–50 cm^{-1} region of the Raman spectrum of monoclinic $\{Cu[Hg(SCN)_4]\}_n$.

absorption band corresponding to the Hg–S stretching mode was reported in the case of orthorhombic $\{Cu[Hg(SCN)_4]\}_n$, while similar stretching modes were reported as medium absorption bands at 213, 216, 219 and 217 cm^{-1} for $Mn[Hg(SCN)_4]$, $Fe[Hg(SCN)_4]$, $Co[Hg(SCN)_4]$ and $Zn[Hg(SCN)_4]$, respectively [76]. The vibration spectrum of orthorhombic $\{Cu[Hg(SCN)_4]\}_n$ below 200 cm^{-1} has not been studied; however, a very strong broad absorption band in the far-IR spectrum of the present (monoclinic) polymorph was observed at 177 cm^{-1}. In contrast, strong absorption bands below 200 cm^{-1}, have been reported at 166 and

124 cm^{-1} for $K_2[Hg(SCN)_4]$ [74]. Lattice vibrations are expected to occur at frequencies around 100 cm^{-1} [79].

The CN stretching region and 400–50 cm^{-1} region of the Raman spectrum are shown in Fig. 7. In the Raman spectrum, the CN stretching is observed as a very asymmetric strong doublet peak at 2168 and 2149 cm^{-1}. The ν_{CS} vibrations occur as very weak bands at 795 and 756 cm^{-1}. The higher energy bending vibration mode of SCN in the Raman spectrum is observed at 467 cm^{-1}, comparable with the one found in the IR spectrum. However, the band at 436 cm^{-1} in the IR spectrum splits to a very weak doublet at 442 and 435 cm^{-1} in the Raman spectrum. The corresponding $2\delta_{SCN}$ vibrations appear as very weak bands at 930 and 888 cm^{-1}. Moreover, the corresponding Cu–N stretching bands in the far-IR spectrum are not detected in the Raman spectrum and a new weak absorption is observed at 273 cm^{-1}. Another new band appears at 244 cm^{-1}. The Hg–S stretching bands were observed as a weak band at 211 cm^{-1}.

4.4. Optical properties, band structure and density of states

A ligand-to-metal charge transfer (LMCT) band at 430 nm has been reported to dominate the UV–vis spectrum of previously reported orthorhombic $\{Cu[Hg(SCN)_4]\}_n$ together with a *d–d* transition at approximately 660 nm [48]. In contrast to this, the tetragonal $(Cu_xZn_{1-x})[Hg(SCN)_4]$ $(0 < x < 0.22)$ is reported to exhibit two intense charge transfer bands at about 330 and 550 nm [48].

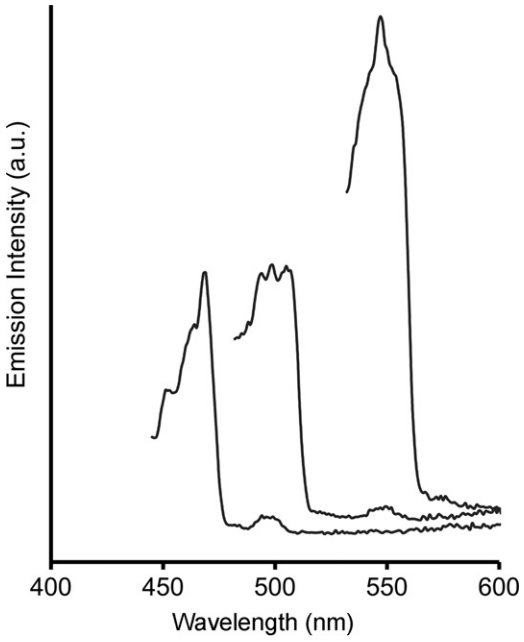

Fig. 8. Emission spectra of monoclinic $\{Cu[Hg(SCN)_4]\}_n$.

Emission spectra of the herein described monoclinic $\{Cu[Hg(SCN)_4]\}_n$ is shown in Fig. 8. In the excitation spectrum, three bands were observed with maxima at 425, 462 and 511 nm. In the emission spectrum, upon excitation at 425 nm, an intense narrow peak appears at 469 nm with two shoulders at 451 and 464 nm. Excitation at 462 nm, results in three narrow peaks with maxima at 494, 499 and 505 nm while excitation at 511 nm leads to one very intense emission band at 547 nm, with two shoulders at 543 and 553 nm.

The calculated band structure of the compound along high symmetry points of the first Brillouin zone is plotted in Fig. 9, where the labeled *k* points are present as L (−0.5, 0.0, −0.5), M (−0.5, −0.5, −0.5), A (−0.5, 0.0, 0.0), G (0.0, 0.0, 0.0), Z (0.0, −0.5, −0.5), V (0.0, 0.0, −0.5). It is found that the top of the valence bands (VBs) has a small dispersion, whereas the bottom of the conduction bands (CBs) exhibit a big dispersion. The lowest energy (2.25 eV) of conduction bands (CBs) is localized at the G point, and the highest energy (0.00 eV) of VBs is localized at the M point. According to our calculations, the compound thus shows a semiconducting character with an indirect band gap of 2.25 eV, which is in good agreement with the experimental values of 2.24 eV obtained from emission spectroscopy.

The bands can be assigned according to total and partial densities of states (DOS), as plotted in Fig. 10. The N-2*s* and C-2*s* states, mixing with small contributions of C-2*p* and N-2*p* states, create the VBs localized at about −17.0 eV. Also, the VBs between −14.0 and −12.0 eV are mainly formed by the S-3*s* and C-2*p* states mixing with small amount of C-2*s*, N-2*s* and S-3*p* states. The VBs between −8.0 eV and the Fermi level (0.0 eV) are essentially formed by S-3*p*, Hg-5*d* and Cu-3*d* states mixing with a partial amount of N-2*p* and C-2*p* states, in which the top of VBs (−0.35 eV) mainly originates from S-3*p* state mixing with a small amount of Cu-3*d* and N-2*p* states. The CBs between 2.0 and 5.2 eV are mainly consisting of hybridizations of S-3*p*, C-2*p* and N-2*p* states mixing with a small amount of Hg-6*s* and C-2*s* states.

Accordingly, the origin of the emission bands of the compound may be mainly ascribed to arise from an excited LLCT state. The corresponding excitation promotes electron density from the occupied S-3*p* state (VB) to the unoccupied π^* orbital of the thiocyanate groups (S-3*p*, C-2*p* and N-2*p* states, CB). Small contributions to the excited state come also from a metal-to-ligand charge transfer (MLCT) (Cu-3*d* [VB] to π^*(SCN) [CB].

4.5. EPR studies

The existence of Cu(II) centers in the compound is also supported by the EPR data. The room temperature X-band EPR

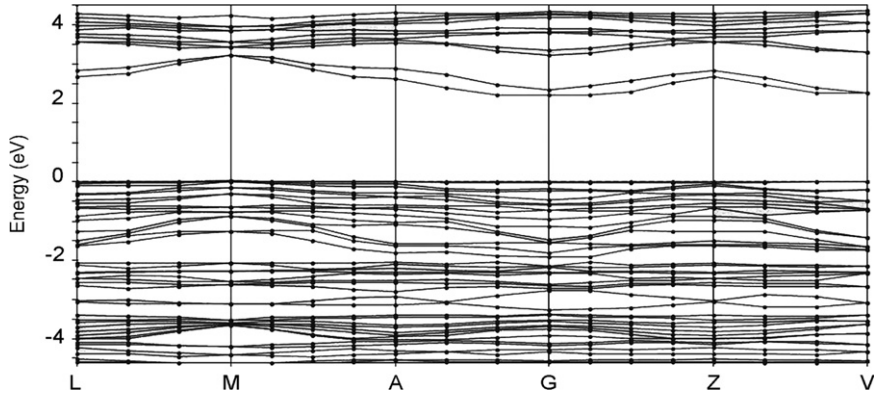

Fig. 9. The band structure of monoclinic $\{Cu[Hg(SCN)_4]\}_n$ (the bands are shown only between −4.5 and 4.5 eV for clarity, and the position of the Fermi level is set at 0 eV).

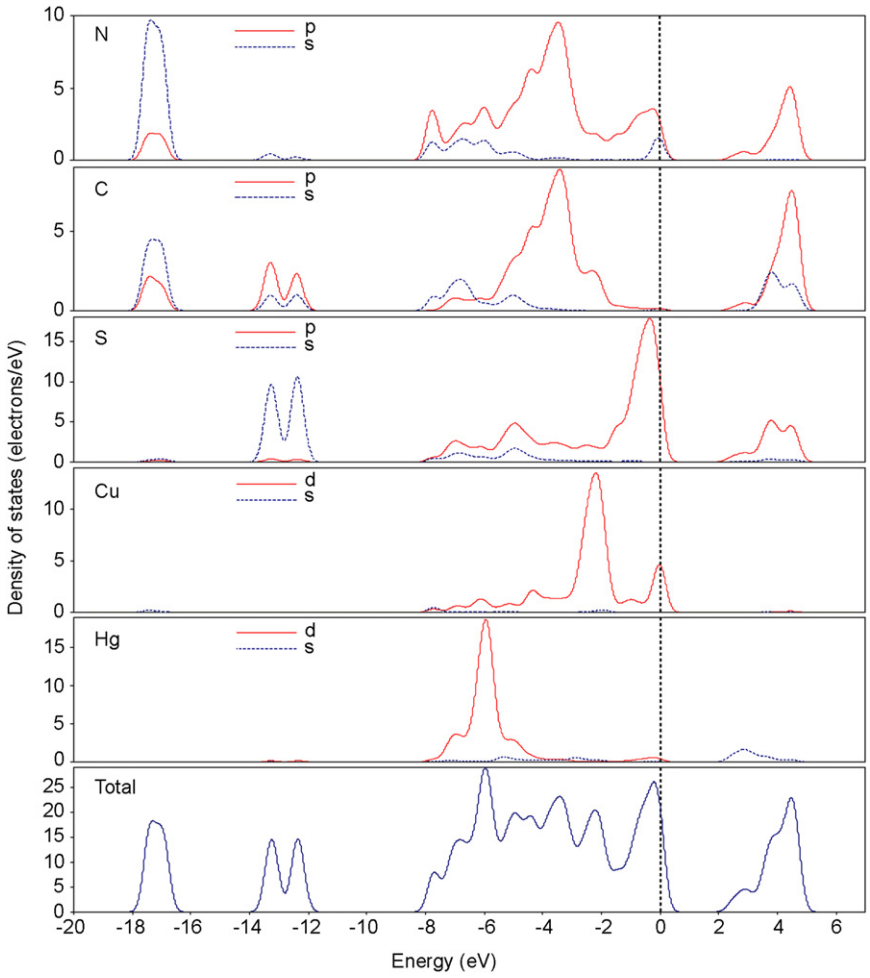

Fig. 10. The total and partial DOS calculated for monoclinic $\{Cu[Hg(SCN)_4]\}_n$. The position of the Fermi level is set at 0 eV.

spectrum of the powdered sample of monoclinic $\{Cu[Hg(SCN)_4]\}_n$ (Fig. 11) reveals an axial signal with anisotropic g factors of $g_\perp=2.0998$ and $g_\parallel=2.2543$. The observed trend of $g_\parallel > g_\perp$ is characteristic of a tetragonal Cu(II) complex with the unpaired d electron in the $d_{x^2-y^2}$ orbital. The measured EPR data is in good agreement with the observed geometry around copper atoms. The $d_{x^2-y^2}$ orbital on the Cu(II) ions, are expected to be directed toward the four in-plane N donors.

In contrast to this, three amalgamated g values of $g_a=2.230$, $g_b=2.065$ and $g_c=2.140$ (determined at 9 GHz, liquid nitrogen temperature) and principle g values of $g_x=2.047$, $g_y=2.065$ and $g_z=2.314$ (35 GHz, at room temperature) are reported for a single crystal of orthorhombic $\{Cu[Hg(SCN)_4]\}_n$ [47].

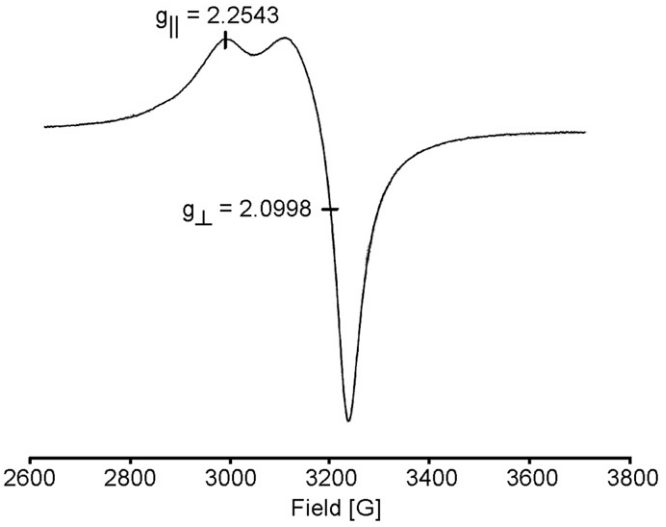

Fig. 11. X band EPR spectrum of monoclinic $\{Cu[Hg(SCN)_4]\}_n$.

5. Conclusions

This study describes a malonate assisted synthesis of the monoclinic polymorph of $\{Cu[Hg(SCN)_4]\}_n$, its crystal structure and luminescence properties. The compound, as determined by X-ray diffraction of a twinned crystal, is a highly porous three dimensional coordination polymer. The electronic band structure along with density of states (DOS) calculated by the DFT method indicates that the compound is an indirect band gap semiconductor. Also, according to the DFT calculations, the luminescence bands of the compound are ascribed to arise from an excited LLCT (p(S) [VB] to π^*(SCN) [CB]) state. Small contributions to the excited state come also from a metal-to-ligand charge transfer (d(Cu) [VB] to π^*(SCN) [CB]) transition.

The comparison of the structural data of the herein reported monoclinic polymorph and the reported orthorhombic derivative reveals no significant structural difference between them. However, we tried to solve and refine the obtained dataset applying the

previously reported *Pbcn*-D_{2h}^{14} [46] and all other orthorhombic space groups; however, neither a rational structure solution was observed nor did the structure converge. The structure was solved in *P*1 and the real space group (*C*2/*c*) was obtained by the ADDSYM algorithm in the program PLATON [56].

Furthermore, IR and Raman measurements reveal decent differences between the newly reported monoclinic $\{Cu[Hg(SCN)_4]\}_n$ and the orthorhombic polymorph reported before. Also, EPR data of a powder sample of the monoclinic polymorph reveals a signal markedly deviating from those observed for the orthorhombic derivative.

Appendix Supplementary material

CCDC 787386 contains the supplementary crystallographic data for the compound. These data can be obtained free of charge from The Cambridge Crystallographic Data Centre via http://www.ccdc.cam.ac.uk/data_request/cif.

Acknowledgments

This study has been supported by the Council of the University of Tabriz, Iran, and the University of Cologne, Germany. The authors thank Dr. Ingo Pantenburg and Mrs. Ingrid Müller for their help with Xray single crystal data collection, Katharina Butsch for her help in crystal structure analysis and Andreas O. Schüren for the EPR measurements.

Appendix A. Supplementary material

Supplementary data associated with this article can be found in the online version at doi:10.1016/j.jssc.2010.12.012.

References

[1] A. Glees, U. Ruschewitz, Z. Anorg. Allg. Chem. 635 (2009) 2046.
[2] Y.-Y. Liu, M. Grzywa, M. Weil, D. Volkmer, J. Solid State Chem. 183 (2010) 208.
[3] T.K. Maji, R. Matsuda, S. Kitagawa, Nat. Mater. 6 (2007) 142.
[4] J.L.C. Rowsell, O.M. Yaghi, J. Am. Chem. Soc. 128 (2006) 1304.
[5] D. Bradshaw, J.B. Claridge, E.J. Cussen, M.J. Rosseinsky, Acc. Chem. Res. 38 (2005) 273.
[6] C.N.R. Rao, S. Natarajan, R. Vaidyanathan, Angew. Chem. Int. Ed. 43 (2004) 1466.
[7] S. Kitagawa, R. Kitaura, S. Noro, Angew. Chem. Int. Ed. 43 (2004) 2334.
[8] R. Robson, S.R. Batten, Angew. Chem. Int. Ed. 37 (1998) 1460.
[9] B.F. Abrahams, A. Hawley, M.G. Haywood, T.A. Hudson, R. Robson, D.A. Slizys, J. Am. Chem. Soc. 126 (2004) 2894.
[10] S. Hu, L. Yun, Y.-Z. Zheng, Y.-H. Lan, A.K. Powell, M.-L. Tong, Dalton Trans. (2009) 1897.
[11] M.A.M. Abu-Youssef, A. Escuer, F.A. Mautner, L. Öhrström, Dalton Trans. (2008) 3553.
[12] M. Eddaoudi, J. Kim, D. Vodak, A. Sudik, J. Wachter, M. O'Keeffe, O.M. Yaghi, PNAS 99 (2002) 4900.
[13] L. Carlucci, G. Ciani, D. Proserpio, Coord. Chem. Rev. 246 (2003) 247.
[14] H. Zhang, D.E. Zelmon, G.E. Price, B.K. Teo, Inorg. Chem. 39 (2000) 1868.
[15] Y. Ling, L. Zhang, J. Li, S.-S. Fan, M. Du, Cryst. Eng. Commun. 12 (2010) 604.
[16] K.M.C. Wong, V.W.W. Yam, Coord. Chem. Rev. 251 (2007) 2477.
[17] D. Braga, F. Grepioni, G.R. Desiraju, Chem. Rev. 98 (1998) 1375.
[18] S. Kitagawa, R. Matsuda, Coord. Chem. Rev. 251 (2007) 2490.
[19] P. Horcajada, C. Serre, M. Vallet-Regi, M. Sebban, F. Taulelle, G. Ferey, Angew. Chem. Int. Ed. 45 (2006) 5974.
[20] A.K. Boudalis, J.M. Clemente-Juan, F. Dahan, J.P. Tuchgues, Inorg. Chem. 43 (2004) 1574.
[21] P. Talukder, A. Datta, S. Mitra, G. Rosair, M. Salah, M.S. El Fallah, J. Ribas, Dalton Trans. (2004) 4161.
[22] F.A. Mautner, R. Vicente, S.S. Massoud, Polyhedron 25 (2006) 1673.
[23] K.-L. Zhang, W. Chen, Y. Xu, Z. Wang, Z.J. Zhong, X.-Z. You, Polyhedron 20 (2001) 2033.
[24] M. Montfort, J. Ribas, X. Solans, Inorg. Chem. 33 (1994) 4271.
[25] R. Vicente, A. Escuer, J. Ribas, X. Solans, J. Chem. Soc. Dalton Trans. (1994) 259.
[26] R. Vicente, A. Escuer, J. Ribas, X. Solans, M. Font-Bardia, Inorg. Chem. 32 (1993) 6117.
[27] J.-P. Zhao, B.-W. Hu, E.C. Sañudo, Q. Yang, Y.-F. Zeng, X.-H. Bu, Inorg. Chem. 48 (2009) 2482.
[28] X.-T. Wang, Z.-M. Wang, S. Gao, Inorg. Chem. 46 (2007) 10452.
[29] T.C. Stamatatos, G.S. Papaefstathiou, L.R. MacGillivray, A. Escuer, R. Vicente, E. Ruiz, S.P. Perlepes, Inorg. Chem. 46 (2007) 8843.
[30] A. Das, G.M. Rosair, M.S. El Fallah, J. Ribas, S. Mitra, Inorg. Chem. 45 (2006) 3301.
[31] S. Paul, R. Clérac, N.G.R. Hearns, D. Ray, Cryst. Growth Des. 9 (2009) 4032.
[32] X. Liu, K.-L. Huang, G.-M. Liang, M.-S. Wang, G.-C. Guo, Cryst. Eng. Commun. 11 (2009) 1615.
[33] M. Wriedt, S. Sellmer, C. Näther, Inorg. Chem. 48 (2009) 6896.
[34] O.V. Nesterova, S.R. Petrusenko, V.N. Kokozay, B.W. Skelton, J. Jezierska, W. Linert, A. Ozarowski, Dalton Trans. (2008) 1431.
[35] A. Rosenheim, E. Cohn, Z. Anorg. Allg. Chem. 27 (1901) 280.
[36] J.G. Bergman, J.J.H. Mcfee, G.R. Crane, Mater. Res. Bull. 5 (1970) 913.
[37] P.N.S. Kumari, S. Kalainathan, N.A.N. Raj, Mater. Lett. 62 (2008) 305.
[38] K.H. He, G. Zheng, G. Chen, T. Lü, M. Wan, G.F. Ji, Physica B 390 (2007) 231.
[39] P.N.S. Kumari, S. Kalainathan, N.A.N. Raj, Mater. Res. Bull. 42 (2007) 2099.
[40] Y.L. Geng, D. Xu, X.Q. Wang, W. Du, H.Y. Liu, G.H. Zhang, Mater. Chem. Phys. 96 (2006) 188.
[41] G.P. Joseph, J. Philip, K. Rajarajan, S.A. Rajasekar, A.J.A. Pragasam, K. Thamizharasan, S.M.R. Kumar, P.J. Sagayaraj, Cryst. Growth 296 (2006) 51.
[42] X.Q. Wang, D. Xu, M.J. Liu, X.Q. Hou, X.F. Cheng, M.K. Lu, D.R. Yuan, J. Huang, Thermochim. Acta 414 (2004) 53.
[43] X. Wang, D. Xu, M. Lu, D. Yuan, G. Zhang, S. Xu, S. Guo, X. Jiang, J. Liu, C. Song, Q. Ren, J. Huang, Y. Tian, Mater. Res. Bull. 38 (2003) 1269.
[44] A. Korczyski, Roczniki Chemii 36 (1962) 1539.
[45] M. Hashimoto, S. Kawai, R. Kiriyama, Bull. Chem. Soc. Jpn. 44 (1971) 2322.
[46] M.A. Porai-Koshits, Zh. Strukt. Khim. 4 (1963) 584.
[47] Y. Kamishina, I. Takada, T. Kanada, J. Phys. Soc. Jpn. 40 (1976) 1787.
[48] D. Forster, D.M.L. Goodgame, Inorg. Chem. 4 (1965) 823.
[49] Y.-Q. Huang, X.-Q. Zhao, W. Shi, W.-Y. Liu, Z.-L. Chen, P. Cheng, D.-Z. Liao, S.-P. Yan, Cryst. Growth Des. 8 (2008) 3652.
[50] D.-L. Long, R.J. Hill, A.J. Blake, N.R. Champness, P. Hubberstery, C. Wilson, M. Schröder, Chem.-Eur. J. 11 (2005) 1384.
[51] M. Casarin, C. Corvaja, C. Di Nicola, D. Falcomer, L. Franco, M. Monari, L. Pandolfo, C. Pettinari, F. Piccinelli, Inorg. Chem. 44 (2005) 6265.
[52] J. Pasán, F.S. Delgado, Y. Rodríguez-Martín, M. Hernández-Molina, C. Ruiz-Pérez, J. Sanchiz, F. Lloret, M. Julve, Polyhedron 22 (2003) 2143.
[53] C. Ruiz-Pérez, Y. Rodríguez-Martín, M. Hernández-Molina, F.S. Delgado, J. Pasán, J. Sanchiz, F. Lloret, M. Julve, Polyhedron 22 (2003) 2111.
[54] Stoe, IPDS Manual, Stoe & Cie GmbH, Germany; X–Red 1.22, Stoe Data Reduction Program, Stoe & Cie GmbH, Germany, 2001.
[55] Y.J. LePage, Appl. Crystallogr. 20 (1987) 264.
[56] A.L. Spek, PLATON, A Multipurpose Crystallographic Tool, Utrecht University, Utrecht, Netherlands, 2001.
[57] G.M. Sheldrick, SHELX-97, Programs for Crystal Structure Analysis, Institüt für Anorganishe Chemie der Universität, Göttingen, Germany, 1998.
[58] WinGX Version 1.70.00, An integrated system of windows programs for the solution, refinement and analysis of single crystal Xray diffraction data, Department of Chemistry, University of Glasgow, 1997–2002;
L.J. Farrugia, J. Appl. Crystallogr. 32 (1999) 837.
[59] R.I. Cooper, R.O. Gould, S. Parsons, D.J. Watkin, J. Appl. Crystallogr. 35 (2002) 168.
[60] S.J. Clark, M.D. Segall, C.J. Pickard, P.J. Hasnip, M.J. Probert, K. Refson, M.C. Payne, Materials Studio CASTEP, version 5.0, Accelrys, San Diego, CA, 2009.
[61] S.J. Clark, M.D. Segall, C.J. Pickard, P.J. Hasnip, M.J. Probert, K. Refson, M.C. Payne, Z. Kristallogr. 220 (2005) 567.
[62] D.R. Hamann, M. Schluter, C. Chiang, Phys. Rev. Lett. 43 (1979) 1494.
[63] B. Rupp, in: M. Sundström, M. Norin, A. Edwards (Eds.), Structural Genomics and High Throughput Structural Biology, Taylor & Francis Group, Boca Raton, 2006, p. 80.
[64] K.N. Bringhurst, D.T. Griffen, Am. Mineral. 71 (1986) 1466.
[65] S. Parsons, Acta Crystallogr. D 59 (2003) 1995.
[66] S. Parsons, in: W. Clegg (Ed.), Crystal Structure Analysis: Principles and Practice, second ed, Oxford University Press, New York, 2009, pp. 271–297.
[67] D.L. Reger, C.A. Little, M.D. Smith, A.L. Rheingold, L.M. Liable-Sands, G.P.A. Yap, I.A. Guzei, Inorg. Chem. 41 (2002) 19.
[68] R.I. Dass, J.B. Goodenough, Phys. Rev. B 67 (2003) 014401.
[69] R.I. Dass, J.-Q. Yan, J.B. Goodenough, Phys. Rev. B 68 (2003) 064415.
[70] J.-W. Cheng, S.-T. Zheng, W. Liu, G.-Y. Yang, Cryst. Eng. Commun. 10 (2008) 1047.
[71] L. Shen, Y.–Z. Xu, J. Chem. Soc. Dalton Trans. (2001) 3413.
[72] G.A.V. Albada, R.A.G. DeDraaff, G.A. Haasnoot, J. Reedjik, Inorg. Chem. 23 (1984) 1404.
[73] K. Nakamoto, Infrared and Raman Spectra of Inorganic and Coordination Compounds, third ed., Wiley, New York, 1978.
[74] R.A. Bailey, S.L. Kozak, T.W. Michelsen, W.N. Mills, Coord. Chem. Rev. 6 (1971) 407.
[75] A. Tramer, J. Chem. Phys. 59 (1962) 232.
[76] D. Forster, D.M.L. Goodgame, Inorg. Chem. 4 (1965) 715.
[77] P.O. Kinell, B. Strandberg, Acta Chem. Scand. 13 (1959) 1607.
[78] M. Julve, M. Verdaguer, G. De Munno, J.A. Real, G. Bruno, Inorg. Chem. 32 (1993) 795.
[79] A. Sabatini, I. Bertini, Inorg. Chem. 4 (1965) 959.